Quantum Frontiers

ORIGINAL ARTICLE Open Access

Moiré induced periodic negative differential conductance on metal bilayer on semiconductor

Jice Sun[1], Shasha Xue[1], Xingsen Chen[1], Ruijun Xi[1], Yi Zhang[1], Xian Du[1], Xuhui Ning[1], Pengyu Hu[1], Tingwen Miao[1], Hao Yang[1,2,3], Hemian Yi[1,2,3], Weijiong Chen[1,2,3], Xiaoxue Liu[1,2,3], Liang Liu[1,2,3], Dandan Guan[1,2,3], Yaoyi Li[1,2,3], Shiyong Wang[1,2,3], Canhua Liu[1,2,3], Hao Zheng[1,2,3*] and Jinfeng Jia[1,2,3,4,5*]

Abstract

Negative Differential Conductance (NDC) is a hallmark anomalous phenomenon in transport measurements, which is relatively rare in scanning tunneling microscopy due to its direct association with the local density of states. In this work, we constructed an ultrathin two-dimensional metal/semiconductor heterostructure by epitaxially growing a bilayer bismuth (Bi) film on a tin selenide (SnSe) substrate, revealing a unique moiré pattern arising from lattice mismatch. Spatially resolved tunneling spectroscopy detected a prominent NDC feature at approximately –650 meV. Both the energy position and depth of the NDC dip are strictly modulated by the periodicity of the moiré pattern. Our work not only establishes a novel Bi/SnSe material platform exhibiting NDC but also reports the visualization of NDC spatially modulated by a two-dimensional moiré superlattice, providing insight for the moiré electronics.

Keywords: Bismuth, Negative differential conductance, Moiré pattern, Scanning tunneling microscopy/spectroscopy

1 Introduction

Negative differential conductance (NDC) refers to an anomalous phenomenon in certain circuits and devices where an increase in voltage leads to a decrease in current. In scanning tunneling microscopy (STM), tunneling conductance typically corresponds to the local density of states (LDOS) of electrons [1–10], which inherently makes the occurrence of NDC particularly challenging. Existing theories suggest that NDC may emerge when weakly connected or weakly coupled conductive systems are present [11, 12]. Previous studies have experimentally observed NDC phenomena in various systems, including self-assembled molecular structures and metal-semiconductor nanojunctions [13–19]. Nevertheless, the NDC phenomenon remains to be further explored and investigated in a broader range of material systems.

When probing electronic states in ultrathin films, measurement results are often modulated by various extrinsic factors, including substrate impurities, surface defects, grain boundaries and strain effects. Specifically, when two periodic lattices are superimposed, moiré patterns can emerge. The resulting moiré potential induces long-range modulation of the electronic band structure, giving rise to phenomena such as half-filling flat bands and second-generation Dirac points [20, 21]. The impact of moiré potential on NDC of the system has become a current research interest.

*Correspondence: haozheng1@sjtu.edu.cn; jfjia@sjtu.edu.cn
[1]State Key Laboratory of Micro-nano Engineering Science, Tsung-Dao Lee Institute & School of Physics and Astronomy, Key Laboratory of Artificial Structures and Quantum Control (Ministry of Education), Shanghai Jiao Tong University, Shanghai 200240, China
[2]Hefei National Laboratory, Hefei 230088, China
Full list of author information is available at the end of the article

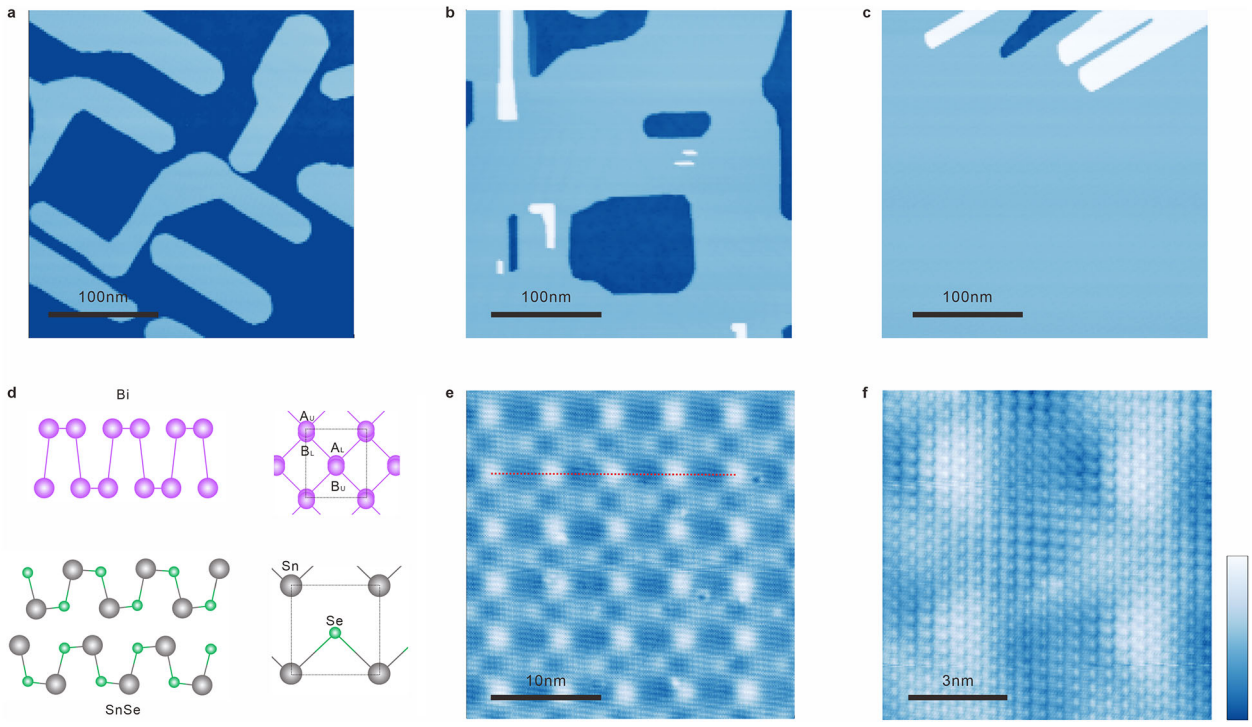

Figure 1 Morphological structure of elementary metal thin film (Bi) grown on semiconductor (SnSe). (a)-(c) Large-scale STM topographic images (300 × 300 nm^2, U = 1 V, I_t = 50 pA) of Bi epitaxially grown on SnSe substrates with coverage of 42.2%, 82.3% and 106%, respectively. (d) Side and top views of crystal structure models of Bi and SnSe. Bismuth, tin and selenium atoms are represented by purple, gray and green spheres, respectively. (e) STM image (30 × 30 nm^2, U = 1 V, I_t = 200 pA) showing the square moiré pattern formed on 1-BL Bi. (f) Atomic-resolution topographic STM image (10 × 10 nm^2, U = 160 mV, I_t = 1 nA) of the square moiré pattern

In this work, we constructed a bilayer metal-semiconductor heterojunction system by epitaxially growing bismuth (Bi) thin films on tin selenide (SnSe) substrate. STM investigations revealed the emergence of moiré patterns in topographic measurements and the observation of NDC in spectroscopic studies. Furthermore, the moiré potential modulates the electronic band structure, endowing the NDC dip with a spatial periodicity that matches the moiré pattern. Our work uncovers a novel material system exhibiting NDC, paving the way for investigating the mutual interplay between NDC and moiré patterns.

2 Results and discussions

Metals typically form islands or clusters when deposited on semiconductor substrates, primarily due to significant differences in chemical bonding, lattice constants, and crystal structures. However, recent studies have revealed that Bi can grow into atomically flat thin films on SnSe substrates [22]. Here, we systematically investigate the coverage dependent morphology of Bi/SnSe system. Clean and atomically flat SnSe (001) surfaces were obtained by performing cleavage in an ultrahigh vacuum (UHV) environment. Via molecular beam epitaxy (MBE), we prepared Bi thin films on SnSe. Figure 1(a) to 1(c) present large-scale STM topographies of our samples. In Fig. 1(a) with the coverage of 42.2%, isolated Bi islands were developed on the SnSe substrate, leaving large areas of bare SnSe exposed. In Fig. 1(b), with a longer deposition time for 82.3% coverage, the isolated Bi islands gradually coalesce into continuous films, accompanied by the appearance of a small number of second-layer Bi regions. In Fig. 1(c), the Bi coverage becomes nearly complete with 106% coverage, forming a largely continuous bilayer with only a few remaining exposed substrate regions and sporadic second-layer Bi patches. The height of Bi film is approximately 580 pm, consistent with one bilayer (1-BL) Bi(110). Repetitive STM topographic characterizations consistently demonstrated the formation of uniform Bi films with large-area and high-quality on the SnSe substrate. SnSe is a kind of group-IV monochalcogenide semiconductors with a moderate bandgap of approximately 1 eV [23], while Bi is typical semimetal with topologically nontrivial bands [24–27]. The reason that Bi wets SnSe is probably mainly due to the shared crystal structure between them, i.e. both Bi and SnSe exhibit a layered structure with interlayer van der Waals bonding. Figure 1(d) illustrates the crystal structure of Bi and SnSe, where the subscripts U and L label the upper and

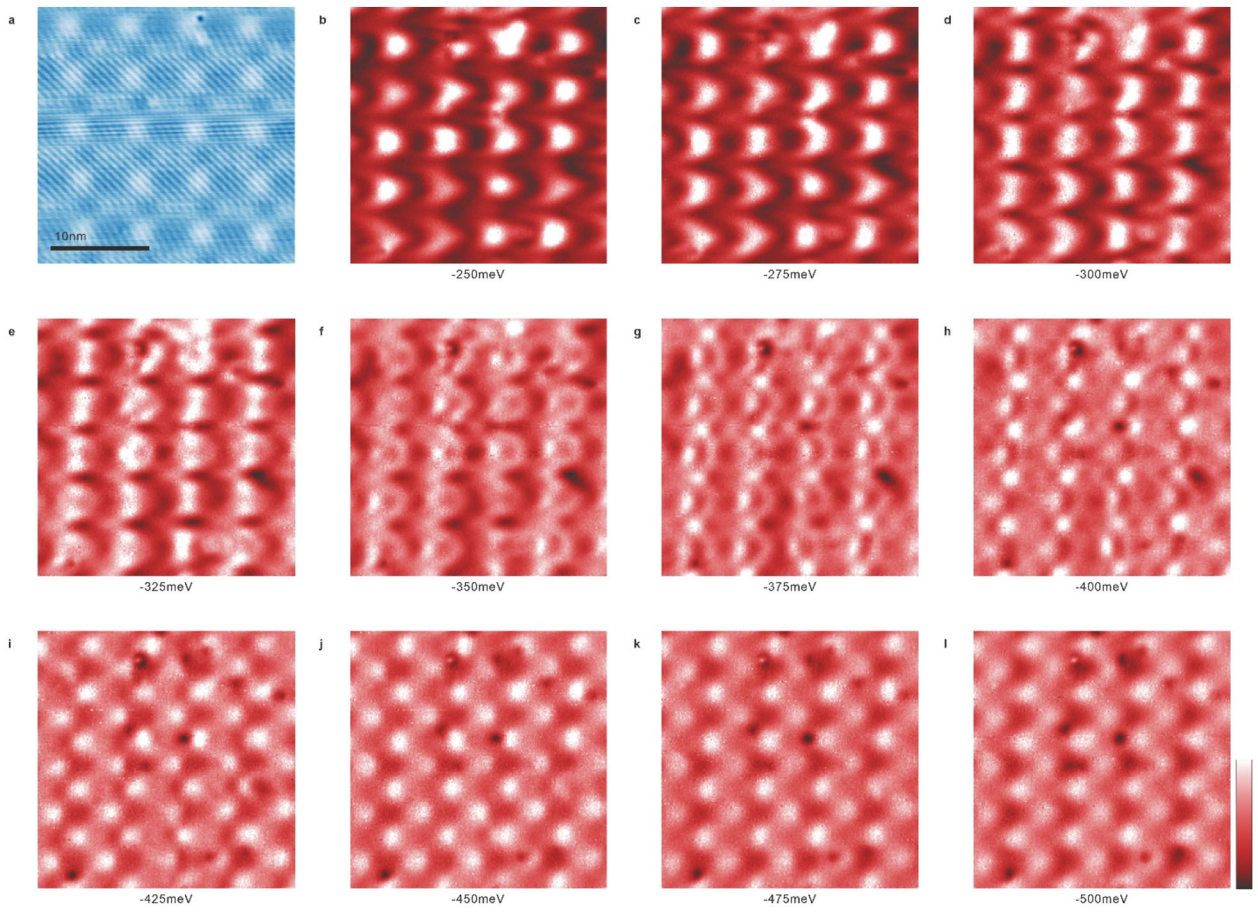

Figure 2 The bias-dependent *dI/dV* maps on a moiré pattern region. (a) STM topography on a moiré pattern region (26 × 26 nm^2, U = 1 V, I_t = 300 pA). (b)-(l), *dI/dV* maps (setpoint: $\mathbf{U}$ = –600 mV, $\mathbf{I_t}$ = 300 pA) taken acquired within the energy range of –250 meV to –500 meV in the region of (a). At the lattice sites corresponding to the highest points of the square moiré pattern, the spatial distribution of the LDOS exhibits a pronounced energy dependence. At an energy of –250 meV, it manifests as solid spheres with a high LDOS. This evolves into hollow rings at –350 meV, and further transforms into solid dark spots with a significantly reduced LDOS at –500 meV

lower atomic sublayers of 1-BL Bi, respectively. Both Bi and SnSe have orthorhombic lattice structures with similar lattice constants. Figure 1(e) displays a medium-scale (30 nm × 30 nm) STM topography of the 1-BL Bi region, where square moiré patterns are clearly observed on the bilayer Bi film. The measured moiré lattice constants along the two principal directions are (5.58 nm, 5.09 nm), respectively, with an interaxial angle of 88° — exhibiting a slight deviation from the ideal square lattice configuration. Figure 1(f) presents atomically resolved STM topographic images that simultaneously reveal both the Bi lattice structure and the coexisting square moiré patterns. The lattice constants of Bi determined by experiment are (495 pm, 444 pm), while the periodicity of the square moiré patterns is approximately ten times that of the Bi lattice.

Subsequently, we investigate the energy-dependent electronic states at the square moiré patterns. Figure 2(a) presents an STM topography of a smaller square moiré pattern region containing a 4 × 5 array of moiré unit cells. Figure 2(b) to 2(l) display spatially resolved local density of states (LDOS) maps acquired in the same region, spanning an energy range from –250 meV to –500 meV. With reference to the moiré unit cell positions marked in Fig. 2(a), the real-space distribution of the LDOS in the square moiré pattern region exhibits pronounced variations at different energies. At a low energy of –250 meV, the map of LDOS at the highest points of the square moiré pattern manifests as solid spheres with a high LDOS. As the energy shifts further away from the Fermi level to –350 meV, this evolves into a hollow ring structure with suppressed LDOS at the center and enhanced LDOS at the periphery. This feature eventually transforms into solid dark spots with significantly reduced LDOS at –500 meV.

Square moiré patterns were observed on the 1-BL Bi film surface, accompanied by a novel periodic oscillation in real-space topographic height. Concurrently, the moiré

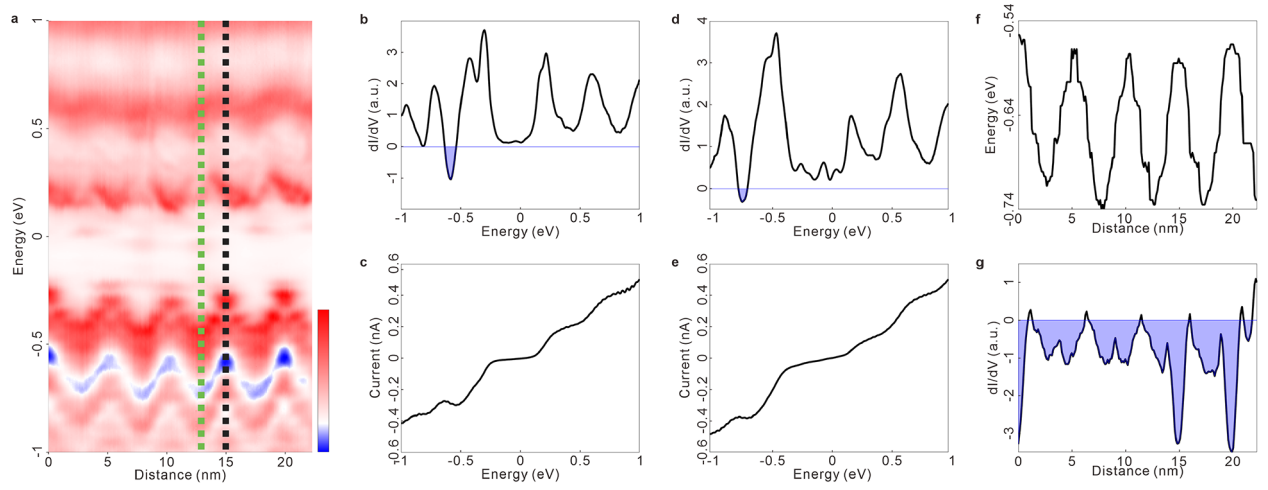

Figure 3 Moiré modulations on the electronic structures and NDC on the moiré pattern of 1-BL Bi. (a) Position-dependent *dI/dV* spectrum (setpoint: U = 1 V, $\mathbf{I_t}$ = 500 pA, $\mathbf{U_{mod}}$ = 20 mV) acquired along the red line in Fig. 1(e). The color represents the LDOS intensity, with red (blue) indicating positive (negative) LDOS values. (b) Differential conductance and (c) tunneling current spectra measured at the position with maximum NDC dip energy indicated as the dash black line in Fig. 3(a). (d) Differential conductance and (e) tunneling current spectra measured at the position with minimum NDC dip energy indicated as the dash green line in Fig. 3(a). (f) Position-dependent energy variation of the NDC dip extracted from the line spectrum in Fig. 3(a). (g) Position-dependent dip value variation of the NDC dip extracted from the line spectrum in Fig. 3(a)

potential was found to modulate the electronic band structure of 1-BL Bi grown on the SnSe substrate, inducing a corresponding periodic oscillation in the band structure across real space. We proceeded to experimentally investigate the spatial characteristics of electronic properties within the square moiré patten region. A position-dependent dI/dV spectrum spanning an energy range of ± 1 eV relative to the Fermi level was obtained in Fig. 3(a), where the color scale represents the spatial variation of LDOS. For clarity, positive dI/dV values are displayed in red, while negative values are represented in blue. The spectrum was initiated from the apex of one moiré topographic unit cell and extended across five consecutive moiré lattice sites as indicated by the red solid line in Fig. 1(e). Modulated by the moiré potential, the electronic band structure of the 1-BL Bi/SnSe system exhibits real-space oscillations with the same periodicity as the moiré pattern. More strikingly, an NDC dip emerges around −650 meV, exhibiting periodic oscillations with real-space position, as clearly demonstrated by the blue band in Fig. 3(a). The values of NDC reach their minima at the moiré lattice sites, with the local NDC minima varying across different lattice sites. Figure 3(b) and 3(c) show the energy-dependent differential conductance and tunneling current spectra measured at the position with maximum NDC dip energy, while Figs. 3(d) and 3(e) present the corresponding spectra acquired at another position exhibiting minimum NDC dip energy. We then systematically extracted the position-dependent characteristics of the NDC dip from the position dependent dI/dV spectra. The moiré spatial modulation affects the NDC not only in the energy positions of the NDC dips but also in their amplitude magnitudes. Figure 3(f) depicts the energy position of the NDC dip as a function of real-space location. The NDC dip appears within an energy range of approximately −600 to −700 meV, with its oscillation period matching that of the moiré pattern. Similarly, Fig. 3(g) shows the amplitude variation of the NDC dip as a function of real-space position. The dip depth exhibits position-dependent modulation within one moiré unit cell, with the maximum NDC dip amplitude occurred at the moiré lattice sites and complete suppression of NDC observed at specific locations. To our best knowledge, this is the first time to observe the moiré induced NDC.

We notice that recent research has described the differential conductance of a STM measurement by following formula [28]:

$$\frac{dI}{dV} = \frac{e^2}{h} T\left(E_F + eV\right) + \frac{e}{h}\int_{E_F}^{E_F+eV} \frac{\partial T}{\partial V} dE$$

where e is the charge of an electron, h is Planck constant, E_F is the Fermi level of sample, and T is the transmission coefficient, which is proportional to the LDOS of the sample. Based on the formula, we suggest a possible interpretation of the NDC observed in our experiment. $\frac{\partial T}{\partial V}$ describes the slope of LDOS. On the descending part of a sharp LDOS peak, $\frac{\partial T}{\partial V}$ becomes negative and may lead to a negative value of dI/dV signal if the peak is sharp enough. In our Bi/SnSe moiré system, if the LDOS round −0.5 eV is

sharp enough to give a negative $\frac{\partial T}{\partial V}$, we could understand the appearance of NDC. Moreover, moiré potential may spatially modulate the LDOS by changing its peak's energies and slopes, which leads to the periodic oscillation of our observed NDC pattern.

In summary, we have successfully grown Bi thin films on SnSe substrates and observed a square moiré pattern on 1-BL Bi. Spatially resolved scanning tunneling spectroscopy (STS) reveals moiré-period-modulated electronic band structures. An NDC dip is observed at approximately −650 meV, with both its depth and energy position being modulated by the moiré periodicity. Our work reveals the existence of a moiré-periodicity-modulated NDC dip, establishing a fundamental framework for investigating the interaction mechanisms between NDC and moiré patterns.

3 Methods

The SnSe (doped with Br at a concentration of 3%) crystals were cleaved in an ultrahigh vacuum system. Bi was then deposited on SnSe by molecular beam epitaxy using a standard Knudsen cell with 99.9999% purity Bi source, while the substrate was kept at room temperature. The base pressure was lower than 2×10^{-10} Torr. After the sample growth was completed, the samples were transferred in situ to the STM for further measurements.

The STM measurements were performed using a commercial STM operating in an ultrahigh vacuum ($\sim 3 \times 10^{-11}$ mBar) environment. The operating temperature was maintained at approximated 7 K with a cryogen-free cooling system. The STM tip was fabricated by electrochemical etching of a tungsten wire (diameter: 0.375 mm), followed by electron-beam cleaning to remove surface oxide layers and subsequent modification via Ag-island. The tunneling differential conductance signal was acquired by standard lock-in technique, where 10-20 mV, 977 Hz were chosen as modulation bias and frequency.

Author contributions

JS did the STM experiments with the help of SX, XC, RX, XD, YZ, XN, TM, PH, HY, HY, WC, DG, XL, LL, YL, SW and CL. HZ and JJ supervise the project. JS wrote the manuscript with contributions from all authors. All authors read and approved the final manuscript.

Funding information

We thank NSFC(Grants No.12488101, No. 92365302, No. 22325203, No. 12474156, No. 12474121, No. 92577203, No. 12574146, No.12574174), the Ministry of Science and Technology of China (Grants No. 2024YFA1410100, No. 2025YFE0201200), the Science and Technology Commission of Shanghai Municipality (Grants No. 2019SHZDZX01, No.24LZ1401000), Cultivation Project of Shanghai Research Center for Quantum Sciences (Grant No. LZPY2024-04), Pujiang Talent Program (Grants No. 24PJA042 and No. 24PJA062) and Quantum Science and Technology-National Science and Technology Major Project (Grant No. 2021ZD0302500) for financial support.

Data availability

All data generated or analyzed during this study are included in this article.

Declarations

Ethics approval and consent to participate

Not applicable.

Consent for publication

Not applicable.

Competing interests

Jin-feng Jia is the Executive Editor for Quantum Frontiers and was not involved in the editorial review, or the decision to publish this article. All authors declare that there are no competing interests.

Author details

[1]State Key Laboratory of Micro-nano Engineering Science, Tsung-Dao Lee Institute & School of Physics and Astronomy, Key Laboratory of Artificial Structures and Quantum Control (Ministry of Education), Shanghai Jiao Tong University, Shanghai 200240, China. [2]Hefei National Laboratory, Hefei 230088, China. [3]Shanghai Research Center for Quantum Sciences, 99 Xiupu Road, Shanghai 201315, China. [4]Quantum Science Center of Guangdong-Hong Kong-Macao Greater Bay Area (Guangdong), Shenzhen 518045, China. [5]Department of Physics, Southern University of Science and Technology, Shenzhen 518055, China.

Received: 12 January 2026 Revised: 9 February 2026
Accepted: 1 March 2026 Published online: 17 March 2026

References

1. C. Bai, *Scanning Tunneling Microscopy and Its Application* (Springer, Berlin, 2000)
2. H. Huang, J. Shen, J. Chen, Q. Shen, G. Lin, Z. Zhu, J. Wu, J. Ma, H. Yang, X. Liu, L. Liu, D. Guan, S. Wang, Y. Li, C. Liu, H. Zheng, Y. Lu, J. Jia, Controllable phase transition of two-dimensional ferromagnetic chromium telluride thin films grown by molecular beam epitaxy. Quantum Front. **2**, 12 (2023). https://doi.org/10.1007/s44214-023-00037-x
3. B. Yang, C. Zhao, B. Xia, H. Ma, H. Chen, J. Cai, H. Yang, X. Liu, L. Liu, D. Guan, S. Wang, Y. Li, C. Liu, H. Zheng, J. Jia, Interface-enhanced superconductivity in monolayer 1T′-$MoTe_2$ on $SrTiO_3$(001). Quantum Front. **2**, 9 (2023). https://doi.org/10.1007/s44214-023-00034-0
4. G. Liu, T. Yang, Y.-X. Jiang, S. Hossain, H. Deng, M.Z. Hasan, J.-X. Yin, Perspective: imaging atomic step geometry to determine surface terminations of Kagome materials and beyond. Quantum Front. **3**, 19 (2024). https://doi.org/10.1007/s44214-024-00066-0
5. Y. Liu, Y. Gu, T. Bao, N. Mao, S. Jiang, L. Liu, D. Guan, Y. Li, H. Zheng, C. Liu, K. Watanabe, T. Taniguchi, W. Duan, J. Jia, S. Jiang, X. Liu, Y. Zhang, T. Li, C. Li, S. Wang, Real-space study of monolayer hBN encapsulated bilayer $MoTe_2$ devices. Quantum Front. **4**, 13 (2025). https://doi.org/10.1007/s44214-025-00086-4
6. Q. Yu, Y. Liu, Y. Yang, D. Liu, S. Xue, X. Chen, R. Xi, J. Sun, X. Du, Y. Zhang, X. Ning, T. Miao, P. Hu, W. Luo, H. Yang, et al., Spectroscopy on superconductor surface modulated by periodic nanostructures. Quantum Front. **4**, 3 (2025). https://doi.org/10.1007/s44214-025-00076-6
7. S. Ding, D. Zhao, T. Jiang, H. Wang, D. Feng, T. Zhang, Surface structure and multigap superconductivity of V_3Si (111) revealed by scanning tunneling microscopy. Quantum Front. **2**, 3 (2023). https://doi.org/10.1007/s44214-023-00028-y
8. W. Liu, Q. Hu, X. Wang, Y. Zhong, F. Yang, L. Kong, L. Cao, G. Li, Y. Peng, K. Okazaki, T. Kondo, C. Jin, J. Xu, H.-J. Gao, H. Ding, Tunable vortex Majorana modes controlled by strain in homogeneous LiFeAs. Quantum Front. **1**, 20 (2022). https://doi.org/10.1007/s44214-022-00022-w
9. H.-K. Xu, F. Li, F.-C. Fei, L. Wang, Y.-S. Gu, D. Liu, Q.-Y. Yu, S.-S. Xue, K. Peng, B. Chen, H.-K. Xie, Z. Zhu, D.-D. Guan, S.-Y. Wang, et al., Visualization of rotational symmetry breaking electronic states in $MnBi_2Te_4$ and $MnBi_4Te_7$. Quantum Front. **1**, 5 (2022). https://doi.org/10.1007/s44214-022-00005-x
10. Z. Zhu, M. Papaj, X.-A. Nie, H.-K. Xu, Y.-S. Gu, X. Yang, D. Guan, S. Wang, Y. Li, C. Liu, J. Luo, Z.-A. Xu, H. Zheng, L. Fu, J.-F. Jia, Discovery of segmented Fermi surface induced by Cooper pair momentum. Science **374**, 1381–1385 (2021). https://doi.org/10.1126/science.abf1077
11. N.D. Lang, Negative differential resistance at atomic contacts. Phys. Rev. B **55**, 9364–9366 (1997). https://doi.org/10.1103/PhysRevB.55.9364
12. Y. Xue, S. Datta, S. Hong, R. Reifenberger, J. Henderson, C. Kubiak, Negative differential resistance in the scanning-tunneling spectroscopy of organic

molecules. Phys. Rev. B **59**, R7852–R7855 (1999). https://doi.org/10.1103/PhysRevB.59.R7852
13. I.K. Song, J.E. Lyons, M.A. Barteau, Correlation of alkane oxidation performance with STM and tunneling spectroscopy measurements of heteropolyacid catalysts. Catal. Today **81**, 137–148 (2003). https://doi.org/10.1016/S0920-5861(03)00107-X
14. D. Steiner, T. Mokari, U. Banin, O. Millo, Electronic structure of metal-semiconductor nanojunctions in gold CdSe nanodumbbells. Phys. Rev. Lett. **95**, 056805 (2005). https://doi.org/10.1103/PhysRevLett.95.056805
15. Y. Podgorny, K. Vorotilov, A. Sigov, Negative differential conductivity in thin ferroelectric films. Appl. Phys. Lett. **105**, 182904 (2014). https://doi.org/10.1063/1.4901317
16. S.Y. Quek, J.B. Neaton, M.S. Hybertsen, E. Kaxiras, S.G. Louie, Negative differential resistance in transport through organic molecules on silicon. Phys. Rev. Lett. **98**, 066807 (2007). https://doi.org/10.1103/PhysRevLett.98.066807
17. H.-J. Müssig, D. Krüger, S. Hinrich, P.O. Hansson, Negative-differential conductivity measured on a germanium layer on Si(001). Surf. Sci. **314**, L884–L888 (1994). https://doi.org/10.1016/0039-6028(94)90222-4
18. S. Loth, M. Wenderoth, L. Winking, R.G. Ulbrich, S. Malzer, G.H. Döhler, Probing semiconductor gap states with resonant tunneling. Phys. Rev. Lett. **96**, 066403 (2006). https://doi.org/10.1103/PhysRevLett.96.066403
19. M.K.-J. Johansson, S.M. Gray, L.S.O. Johansson, Studies of low coverage adsorption of Li on Si(001): observation of negative differential resistance and electron trapping. J. Vac. Sci. Technol., B Microelectron. Nanometer Struct. Process. Meas. Phenom. **14**, 1015–1018 (1996). https://doi.org/10.1116/1.588445
20. J.R. Wallbank, A.A. Patel, M. Mucha-Kruczyński, A.K. Geim, V.I. Fal'ko, Generic miniband structure of graphene on a hexagonal substrate. Phys. Rev. B **87**, 245408 (2013). https://doi.org/10.1103/PhysRevB.87.245408
21. Y. Cao, V. Fatemi, S. Fang, K. Watanabe, T. Taniguchi, E. Kaxiras, P. Jarillo-Herrero, Unconventional superconductivity in magic-angle graphene superlattices. Nature **556**, 43–50 (2018). https://doi.org/10.1038/nature26160
22. Q. Lu, P.V.S. Reddy, H. Jeon, A.R. Mazza, M. Brahlek, W. Wu, S.A. Yang, J. Cook, C. Conner, X. Zhang, A. Chakraborty, Y.-T. Yao, et al., Realization of a two-dimensional Weyl semimetal and topological Fermi strings. Nat. Commun. **15**, 6001 (2024). https://doi.org/10.1038/s41467-024-50329-6
23. C. Yue, Z. Huang, W.-L. Wang, Z. Gao, H. Lin, J. Liu, K. Chang, Identification and manipulation of atomic defects in monolayer SnSe. ACS Nano **18**, 25478–25488 (2024). https://doi.org/10.1021/acsnano.4c04789
24. H.-H. Sun, M.-X. Wang, F. Zhu, G.-Y. Wang, H.-Y. Ma, Z.-A. Xu, Q. Liao, Y. Lu, C.-L. Gao, Y.-Y. Li, C. Liu, D. Qian, D. Guan, J.-F. Jia, Coexistence of topological edge state and superconductivity in bismuth ultrathin film. Nano Lett. **17**, 3035–3039 (2017). https://doi.org/10.1021/acs.nanolett.7b00365
25. F. Yang, L. Miao, Z.F. Wang, M.-Y. Yao, F. Zhu, Y.R. Song, M.-X. Wang, J.-P. Xu, A.V. Fedorov, Z. Sun, G.B. Zhang, et al., Spatial and energy distribution of topological edge states in single Bi(111) bilayer. Phys. Rev. Lett. **109**, 016801 (2012). https://doi.org/10.1103/PhysRevLett.109.016801
26. C. Liu, S. Tao, G. Wang, H. Chen, B. Xia, H. Yang, X. Liu, L. Liu, Y. Li, S. Wang, H. Zheng, C. Liu, D. Guan, Y. Lu, J. Jia, Tunable topological edge states in black-phosphorus-like Bi(110). Phys. Rev. B **110**, 195427 (2024). https://doi.org/10.1103/PhysRevB.110.195427
27. G. Wang, L.-S. Liu, Z. Zhu, Y. Zheng, B. Yang, D. Guan, S. Wang, Y. Li, C. Liu, W. Chen, H. Zheng, J. Jia, Quantum-size effect induced Andreev bound states in ultrathin metallic islands proximitized by a superconductor. Phys. Rev. Lett. **135**, 076201 (2025). https://doi.org/10.1103/4mw4-4rfh
28. S.-Y. Li, H. Liu, J.-B. Qiao, H. Jiang, L. He, Magnetic-field-controlled negative differential conductance in scanning tunneling spectroscopy of graphene npn junction resonators. Phys. Rev. B **97**, 115442 (2018). https://doi.org/10.1103/PhysRevB.97.115442

Publisher's note